Journal of Sound and Vibration (2000) **235**(1), 25–42
doi:10.1006/jsvi.1999.2912, available online at http://www.idealibrary.com on IDEAL®

EMISSION OF SOUND FROM TURBULENCE CONVECTED BY A PARALLEL MEAN FLOW IN THE PRESENCE OF A CONFINING DUCT

M. E. GOLDSTEIN

National Aeronautics and Space Administration, Glenn Research Center, Cleveland, OH 44135, *U.S.A.*

AND

S. J. LEIB

Ohio Aerospace Institute, 22800 *Cedar Point Road, Brook Park, OH* 44142, *U.S.A.*

(*Received* 19 *April* 1999, *and in final form* 20 *December* 1999)

An approximate method for calculating the noise generated by a turbulent flow within a semi-infinite duct of arbitrary cross-section is developed. It is based on a previously derived high-frequency solution to Lilley's equation, which describes the sound propagation in a transversely sheared mean flow. The source term is simplified by assuming the turbulence to be axisymmetric about the mean flow direction. Numerical results are presented for the special case of a ring source in a circular duct with an axisymmetric mean flow. They show that the internally generated noise is suppressed at sufficiently large upstream angles in a hard-walled duct, and that acoustic liners can significantly reduce the sound radiated in both the upstream and downstream regions, depending upon the source location and Mach number of the flow.

1. INTRODUCTION

The National Aeronautics and Space Administration has recently made a large investment in the development of a new generation of supersonic transports. A primary design requirement was that the aircraft be quiet enough to meet, or even exceed, existing noise regulations, and it was decided that a mixer-ejector nozzle concept would be used to accomplish this objective. The idea was that a significant amount of the mixing noise would be generated internally within the nozzle, and could therefore be considerably reduced by using suitable acoustic linear designs. When recent tests of a prototype mixer-ejector nozzle revealed that the peak internal turbulence level is more than twice that in the external stream, it was decided that we needed to develop better prediction methods for this internally generated noise. A general theory based on Lighthill's equation had already been developed by Goldstein and Rosenbaum [1] and Dill *et al.* [2] extended this analysis to account for mean-flow refraction effects.

However, both theories involve the solution of a complicated Weiner–Hopf problem, which can only be explicitly worked out for a slug (or "top hat") mean velocity profile.

On the other hand many of the most successful jet noise predictions (e.g., the MGB code [3]) are based on high-frequency Lilley's-equation solution [4], while the mixer-ejector tests showed that the internal noise was of much higher frequency than the externally generated

0022-460X/00/310025 + 18 $35.00/0

noise. We therefore decided to develope a theory based on the high-frequency Lilley's-equation solution.

We assumed that the sound was generated by a superposition of statistically independent and acoustically compact convecting-point quadrupoles and derived a formula for the high-frequency acoustic radiation generated by such sources when they are located within a semi-infinite, parallel-walled nozzle. In fact, we supposed that the mean flow was completely parallel, but allowed the cross-sectional shape and velocity profile to be arbitrary (as shown in Figure 1(a)), in order to account for nozzle-geometry effects. The only variation in the streamwise direction is due to the boundary condition change at the nozzle exit, which was allowed to have an arbitrary shape. Finally, an arbitrary (frequency-dependent) acoustic impedance boundary condition was imposed at the nozzle walls, in order to model an acoustically treated surface. The resulting solutions can then be superimposed to calculate the sound generated by an actual turbulent flow within a nozzle.

While this work was primarily motivated by the need to analyze the internally generated sound produced by a mixer-ejector nozzle, the analysis has many other applications, such as to long-cowl jet engines with forced mixers, the design of effective acoustic liners that may be required to absorb the noise radiated in specific directions, and to the design of nozzle exit shapes that reduce the noise radiation below the flight path.

Goldstein [5, equation (5.9)] developed a formula for the high-frequency sound radiation from a convecting-point quadrupole source in an arbitrary, transversely sheared mean flow. This result was later extended by Durbin [6, 7] to account for a general (not necessarily parallel) mean flow. These formulas involve a ray-spreading factor that multiplies the product of a source function—which describes the actual acoustic sources—with some Doppler factors that account for the local source and mean flow convection effects. The spreading factor accounts for the mean-flow variation along the path of the radiated sound and can be calculated from geometric acoustics, or ray tracing.

The present paper shows that Goldstein's [5] formula still applies to the internally generated noise and that only the ray-tracing analysis, which is used to calculate the ray-spreading factors, needs to be modified in order to account for the effect of the nozzle walls. This is demonstrated in Section 2, where the notation is introduced and the Goldstein [5] and Durbin [6] analyses are reviewed in some detail.

Three-dimensional ray tracing is fairly complex and somewhat difficult to implement numerically, but reference [5] shows that the three-dimensional ray-tracing computation can be reduced to a much simpler two-dimensional calculation for the doubly infinite jet flow considered in that paper. The rays can then be found by solving a single second-order equation. Section 3, shows that this can also be done in the present problem. The results are applied to an actual turbulent flow in section 4 and specialized to an axisymmetric mean flow in a round duct with circular exit plane in section 5, where some numerical results are also presented. Some conclusions and recommendations for further work are given in section 6.

2. EXTENSION OF DOUBLY INFINITE JET SOLUTION TO ACCOUNT FOR FINITE NOZZLE GEOMETRY

For definiteness, we consider a unidirectional, transversely sheared, parallel mean flow:

$$\mathbf{v} = \hat{\mathbf{i}}U(x_t), \quad \rho = \bar{\rho}(\mathbf{x}_t), \quad c = \bar{c}(\mathbf{x}_t), \quad p = \text{constant}, \tag{1}$$

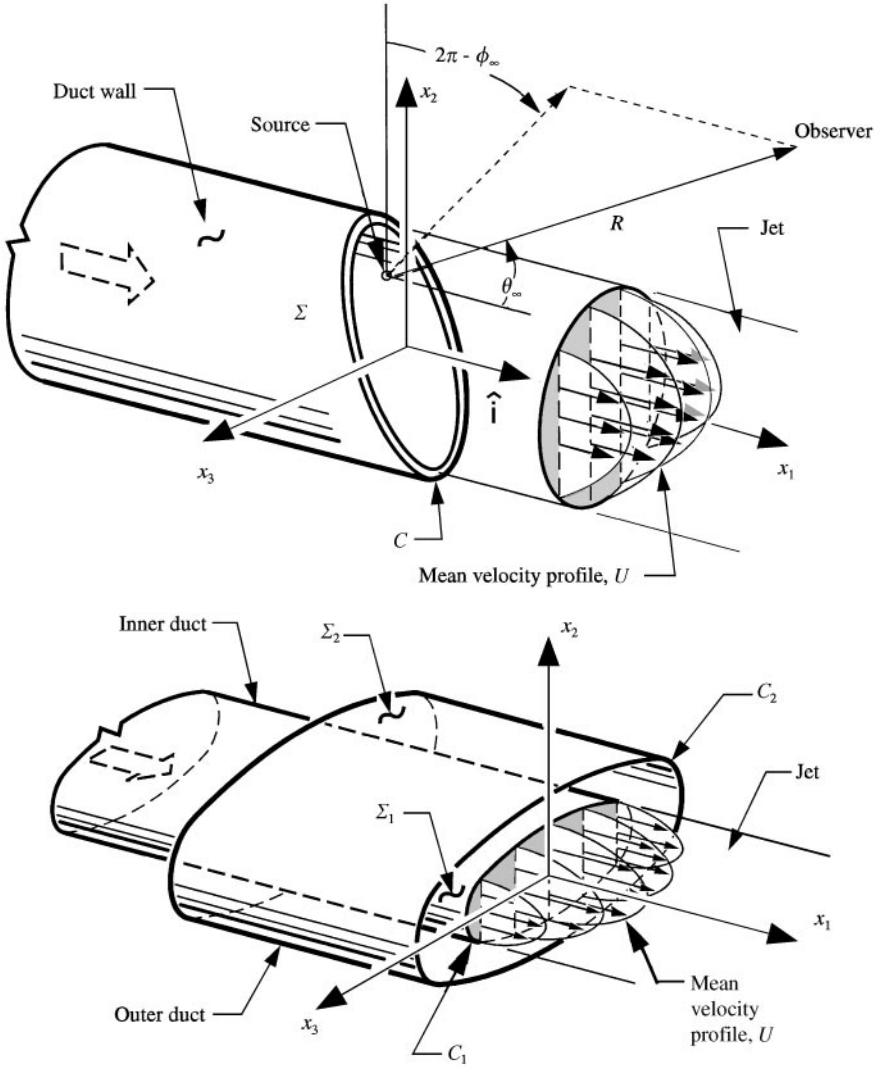

Figure 1. (a) Flow configuration; (b) example of more complex configuration to which analysis applies.

with velocity $\mathbf{v}$, density ρ, speed of sound c, and pressure p, exiting from a parallel-walled nozzle, as shown in Figure 1(a). The result which we obtain, however, is much more general and applies to more complicated flow configurations, such as the one shown in Figure 1(b). Equation (1) is an exact solution of the inviscid, non-heat-conducting equations of motion for these configurations. $\mathbf{x} = \{x_1, x_2, x_3\}$ denote Cartesian co-ordinates with x_1 aligned with the direction of the mean flow, $\hat{\mathbf{i}}$ denotes the unit vector in this direction, and $\mathbf{x}_t = \{x_2, x_3\}$ denotes the transverse coordinate vector. The nozzle exit is described by an arbitrary, three-dimensional curve C, as shown in the figure. The mean velocity U is assumed to go smoothly to zero at the generators of the nozzle wall, and to remain zero beyond that surface. Also, the mean density and speed of sound approach their ambient values at the wall. The analysis does not therefore account for forward flight effects, but can easily be extended to do so.

Assuming that the ideal gas law applies, the linearized equation governing the acoustic propagation on this flow is [8]

$$\mathscr{L}p \equiv \frac{\mathrm{D}}{\mathrm{D}t}\left(\frac{\mathrm{D}^2}{\mathrm{D}t^2} - \nabla\cdot\bar{c}^2\,\nabla p\right) + 2\bar{c}^2\,\nabla U\cdot\nabla\frac{\partial p}{\partial x_1} = \Gamma, \tag{2}$$

where p now denotes the acoustic pressure fluctuation normalized by $\bar{\rho}\bar{c}^2$,

$$\frac{\mathrm{D}}{\mathrm{D}t} \equiv \frac{\partial}{\partial t} + U\,\frac{\partial}{\partial x_1} \tag{3}$$

denotes the convective derivative and t denotes the time. Γ represents the acoustic source distribution and is given by

$$\Gamma = \frac{\mathrm{D}}{\mathrm{D}t}\,\nabla\cdot\mathbf{f} - 2\nabla U\cdot\frac{\partial\mathbf{f}}{\partial x_1}, \tag{4}$$

when this quantity is produced by a fluctuating force f_i per unit volume. In the absence of temperature fluctuations, Lilley's equation is obtained by replacing f_i by the quadrupole source distribution $f_i = \partial u_i u_j/\partial x_j$, where u_i denotes the velocity fluctuation within the flow.

Since the problem is linear, and the second term in equation (4) is negligible compared to the first in the high-frequency limit, the solution for an arbitrary force distribution f_i can be obtained by superposition of solutions, say p_G, to

$$\mathscr{L}\,(p_G\,\mathrm{e}^{-\mathrm{i}\omega t}) = \frac{D}{Dt}\,\delta(\mathbf{x}-\mathbf{x}^s)\,\mathrm{e}^{-\mathrm{i}\omega t}, \tag{5}$$

where ω is the frequency, $\mathbf{x}^s$ denotes the source position, and δ is the Dirac delta function.

2.1. REVIEW OF DURBIN'S HIGH-FREQUENCY SOLUTION

By using matched asymptotic expansions, Durbin [6] showed that the solution to this problem is given by

$$p_G = p_G\,(\mathbf{x}\,|\,\mathbf{x}^s,\omega) = (1 - M\,s_1)\;\Phi\mathrm{e}^{\mathrm{i}kS}, \tag{6}$$

in the high-frequency limit

$$k \equiv \omega/\bar{c}_\infty \to \infty\,, \tag{7}$$

where $\bar{c}_\infty$ is the speed of sound in the region of zero mean flow,

$$M \equiv U/\bar{c}_\infty, \tag{8}$$

S denotes the Eikenal, which satisfies the Eikenal equation

$$(1 - M\,s_1)^2 - \left(\frac{\bar{c}}{\bar{c}_\infty}\right)^2 |\,\mathbf{s}\,|^2 = 0, \tag{9}$$

and

$$\mathbf{s} = \{s_1, s_2, s_3\} \equiv \nabla S. \tag{10}$$

The solution to the first-order partial differential equation (9) can be obtained by the method of characteristics by calculating S along the rays $\mathbf{x}(\tau)$, which are determined by the ordinary differential equations

$$\dot{s}_1 = 0, \quad \dot{x}_1 = s_1 \left[1 - \left(\frac{U}{\bar{c}} \right)^2 \right] + \frac{U \bar{c}_\infty}{\bar{c}^2}, \tag{11, 12}$$

$$\left. \begin{aligned} \dot{x}_i &= s_i \\ \dot{s}_i &= \frac{1}{2} \frac{\partial}{\partial x_i} \left(\frac{s_1 U - \bar{c}_\infty}{\bar{c}} \right)^2 \end{aligned} \right\}, \quad i = 2, 3 \tag{13}$$

subject to the initial conditions at the source position $\mathbf{x}^s$ that the initial ray velocity is proportional to the initial ray direction, say $\{\cos\mu, \sin\mu\cos\lambda, \sin\mu\sin\lambda\}$, i.e., that

$$\dot{\mathbf{x}}_s = \gamma_s \{\cos\mu, \sin\mu\cos\lambda, \sin\mu\sin\lambda\}, \tag{14}$$

where τ is a parameter that varies continuously along the ray, the dot denotes differentiation with respect to τ, the subscript s denotes quantities evaluated at the source position $\mathbf{x}^s$, and the proportionality constant γ_s is given by

$$\gamma_s^{-2} = (\bar{c}_s / \bar{c}_\infty)^2 \left[1 - \left(\frac{U_s}{\bar{c}_s} \sin\mu \right)^2 \right]. \tag{15}$$

The amplitude function Φ is given by

$$\Phi \equiv \frac{1}{4\pi \bar{c} \bar{c}_\infty \ (1 - M_s s_1)} \sqrt{\frac{\gamma^{3s} \sin\mu}{\gamma J}}, \tag{16}$$

where J denotes the Jacobian determinant

$$J = \left| \frac{\partial(x_1, x_2, x_3)}{\partial(\sigma, \mu, \lambda)} \right|, \tag{17}$$

with $\mathrm{d}\sigma = |\mathrm{d}\mathbf{x}|$ denoting the distance along the ray.

Once the ray equations (11)–(13) are solved, the Eikenal can be found by integrating the equation

$$\dot{S} = \mathbf{s} \cdot \dot{\mathbf{x}}, \tag{18}$$

and the velocity fluctuation $\mathbf{u}_G$, corresponding to the normalized acoustic pressure perturbation p_G, can be calculated from

$$\mathbf{u}_G = \bar{c}^2 \, \mathbf{s} \, \Phi \, \mathrm{e}^{\mathrm{i}kS} / \bar{c}_\infty. \tag{19}$$

The important thing to notice is that the derivation of these results is completely independent of any boundary conditions that are imposed on the surface Σ of the duct, and the termination curve C of the duct exit. The latter gives rise to the so-called defracted radiation which [9] is of higher order in frequency than the direct and reflected radiation and can therefore legitimately be neglected in the high-frequency limit.

2.2. MODIFICATION OF SOLUTION TO ACCOUNT FOR THE DUCT WALLS

The conditions at the surface of the duct are accounted for by imposing boundary conditions on the solutions to the ray equations (11) – (13) at the point where the rays reach the boundary to produce a reflected wave, say $\{p_+, u_+\}$, corresponding to the incident wave, say $\{p_-, u_-\}$ (see, for example, Pierce [9]).

The reflected wave is still given by equation (6) with equation (16), but multiplied by a reflection coefficient, say $\mathscr{R}$. The Eikenal S is obtained by integrating equation (18) through the reflection.

Thus, since the Jacobian determinant (and therefore Φ) is continuous across a reflection [10], the pressure and velocity on the boundary Σ are given by

$$p_G = \Phi(1 + \mathscr{R})\, e^{ikS} \tag{20}$$

and

$$\mathbf{u}_G = \bar{c}_\infty\, \Phi(\mathbf{s}_- + \mathscr{R}\mathbf{s}_+)\, e^{ikS} \tag{21}$$

(recall that $U = 0$ and $\bar{c} = \bar{c}_\infty$ at Σ).

The usual impedance boundary condition for a locally reacting surface involves only the normal component of the velocity $\mathbf{u}_G$, and therefore only the normal component of the propagation vector $\mathbf{s}$. This condition is usually expressed in terms of an impedance, say Z (which can, in general, be a function of the frequency ω), as

$$Z = \bar{\rho}_\infty \bar{c}_\infty^2 \frac{p_G}{\mathbf{u}_G \cdot \hat{\mathbf{n}}} \quad \text{for } \mathbf{x} \text{ on } \Sigma, \tag{22}$$

where $\hat{\mathbf{n}}$ denotes the unit normal to Σ. Moreover, the normal component of $\mathbf{s}$ changes sign at a reflection, i.e.,

$$\mathbf{s}_- \cdot \hat{\mathbf{n}} = -\mathbf{s}_+ \cdot \hat{\mathbf{n}} \quad \text{for } \mathbf{x} \text{ on } \Sigma. \tag{23}$$

Substituting this along with equations (20) and (21) into equation (22) yields the expression for the reflection coefficient,

$$\mathscr{R} = \frac{\eta + 1}{\eta - 1}, \tag{24}$$

where

$$\eta \equiv -(\mathbf{s}_- \cdot \hat{\mathbf{n}})\zeta, \tag{25}$$

and $\zeta = Z/\bar{\rho}_\infty \bar{c}_\infty$ is a normalized impedance. Notice that $Z \to \infty$ and $\mathscr{R} \to 1$ for a hard wall.

The tangential components of $\mathbf{s}$ on the other hand remain unchanged by the reflection, and it therefore follows from equation (11) that

$$s_1 = \text{constant}, \tag{26}$$

which is equal to the farfield value of this quantity for any ray that propagates to infinity (which are the only ones we are interested in here). In this region (where the mean flow is zero), the acoustic rays are straight lines and are therefore given by

$$\mathbf{x} = \mathbf{x}^s + R\{\cos\theta_\infty, \sin\theta_\infty \cos\phi_\infty, \sin\theta_\infty \sin\phi_\infty\}, \tag{27}$$

where R can be taken as the distance between the source point and the observation point, and θ_∞ and ϕ_∞ denote the farfield polar and circumferential angles, respectively, shown in Figure 1.

It therefore follows from equations (11)–(13) and the Eikenal equation (18) that $\dot{R} = 1$, and that

$$s_1 = \cos\theta_\infty. \tag{28}$$

The Jacobian determinant (17) becomes

$$J = R^2 \sin\theta_\infty \left| \frac{\partial(\theta_\infty, \phi_\infty)}{\partial(\mu, \lambda)} \right|, \tag{29}$$

and it now follows from equations (12), (14), and (28) that

$$\gamma_s \cos\mu = \left[1 - \left(\frac{U_s}{\bar{c}_s} \right)^2 \right] \cos\theta_\infty + \frac{U_s \bar{c}_\infty}{\bar{c}_s^2}. \tag{30}$$

Eliminating γ_s between this and equation (15) shows that θ_∞ depends only on μ, and not λ, and that

$$\gamma_s^3 \left(\frac{\bar{c}_s}{\bar{c}_\infty} \right)^2 = \frac{\sin\theta_\infty}{\sin\mu} \frac{\mathrm{d}\theta_\infty}{\mathrm{d}\mu}. \tag{31}$$

Inserting this into equation (16) and using equation (29) shows that

$$\Phi \to \frac{1}{4\pi R \bar{c}_s \bar{c}_\infty (1 - M_s \cos\theta_\infty)} \sqrt{\left| \frac{\mathrm{d}\lambda}{\mathrm{d}\phi_\infty} \right|}. \tag{32}$$

It follows from equations (6) and (20) that

$$p_G \to \Phi \bar{\mathscr{R}} \, \mathrm{e}^{\mathrm{i}kS}, \tag{33}$$

where we have put

$$\bar{\mathscr{R}} \equiv \prod_{i=1}^{m} \mathscr{R}_i, \tag{34}$$

and the $\mathscr{R}_i$ denote the individual reflection coefficients for each of the m reflections that the ray undergoes before leaving the duct. Also, it follows from equations (13), (18) and (28) that

$$S = (x_1 - x_1^s) \cos\theta_\infty + S_0(\mathbf{x}_t \,|\, \mathbf{x}_t^s). \tag{35}$$

2.3. APPLICATION TO MOVING POINT SOURCE

As indicated in the Introduction, the sound radiated by an actual turbulent flow can be calculated in terms of the pressure field p generated by superposition of point quadrupole sources moving downstream with the mean flow. We therefore consider the source distribution

$$\Gamma = \frac{\mathrm{D}}{\mathrm{D}t} \frac{\partial^2}{\partial x_i \partial x_j} \mathrm{e}^{-\mathrm{i}\omega_s t} \, \delta(\mathbf{x} - \mathbf{x}_t^s - \hat{\mathbf{i}} U_c t) \, Q_{ij}, \tag{36}$$

where ω_s denotes the source frequency, and U_c is the convection speed of the source, whose strength is Q_{ij}.

The corresponding acoustic field can be calculated from the fixed source solution p_G by superposing Fourier components and using the Green's formula [5]

$$p = \frac{Q_{ij}}{2\pi} \int_{\infty}^{-\infty} \int p_G(\mathbf{x} \mid \mathbf{y}, \omega)\, \mathrm{e}^{-\mathrm{i}\omega(t-\tau)} \frac{\partial^2}{\partial x_i^s \partial x_j^s} \mathrm{e}^{-\mathrm{i}\omega_s \tau}\, \delta(\mathbf{y} - \mathbf{x}_t^s - \hat{\mathbf{i}} U_c \tau)\, \mathrm{d}\mathbf{y}\, \mathrm{d}\tau\, \mathrm{d}\omega. \tag{37}$$

Integrating by parts to transfer the derivatives from the source term to the Green's function, and carrying out the integrations with respect to $\mathbf{y}_t$ and τ gives

$$p = \frac{Q_{ij}}{2\pi U_c} \mathrm{e}^{-\mathrm{i}\omega_s t} \int_{-\infty}^{\infty} \mathrm{e}^{\mathrm{i}(\omega-\omega_s)(x_1^s/U_c - t)} \frac{\partial^2}{\partial x_i^s \partial x_j^s} p_G(\mathbf{x} \mid \mathbf{x}^s, \omega)\, \mathrm{d}x_1^s\, \mathrm{d}\omega. \tag{38}$$

For clarity, we begin with the case where only a single ray reaches the observer. The result will then be corrected for multiple ray effects in a relatively obvious manner. Inserting equations (33) and (35) into equation (38), and using the fact that (at lowest approximation) the partial derivatives operate only on the frequency-dependent terms in the exponent, we obtain

$$p = (1 - M\cos\theta_\infty)\, \mathrm{e}^{-\mathrm{i}\omega_s t} \frac{Q_{ij}}{2\pi U_c} \int_{-\infty}^{\infty} \Phi \bar{\mathscr{R}} \mathrm{e}^{\mathrm{i}(\omega-\omega_s)(x_1^s/U_c - t)} \times \frac{\partial^2}{\partial x_i^s \partial x_j^s} \mathrm{e}^{\mathrm{i}(\omega/\bar{c}_\infty)[(x_1 - x_1^s)\cos\theta_\infty + S_0]}\, \mathrm{d}x_1^s\, \mathrm{d}\omega. \tag{39}$$

Then, carrying out the integration, first with respect to x_1^s (to obtain a δ-function), and then with respect to ω, shows that

$$p = \frac{-(1 - M\cos\theta_\infty)\sigma_i \sigma_j Q_{ij}}{(1 - M_c\cos\theta_\infty)} k_s^2\, \Phi\, \bar{\mathscr{R}} \mathrm{e}^{(\mathrm{i}\omega_s/\bar{c}_\infty(1 - M_c\cos\theta_\infty))(x_1\cos\theta_\infty + S_0 - \bar{c}_\infty t)}, \tag{40}$$

where we have put $M_c = U_c/\bar{c}_\infty$, $k_s = \omega_s/\bar{c}_\infty$ and

$$\sigma_1 = \frac{\cos\theta_\infty}{1 - M_c\cos\theta_\infty}; \quad \sigma_i = \frac{-1}{1 - M_c\cos\theta_\infty} \frac{\partial S_0}{\partial x_i^s}, \quad \text{for } i = 2, 3. \tag{41}$$

Then it follows from equation (32) that

$$|p|^2 \to \frac{k_s^4 |Q_{ij}\sigma_i\sigma_j|^2 |\bar{\mathscr{R}}|^2}{(4\pi R)^2\, \bar{c}_s^2\, \bar{c}_\infty^2\, (1 - M_s\cos\theta_\infty)^2 (1 - M_c\cos\theta_\infty)^2} \left|\frac{\mathrm{d}\lambda}{\mathrm{d}\phi_\infty}\right|, \tag{42}$$

in the far field where $M = 0$, which, except for some minor notational changes, and the inclusion of the reflection coefficient $\bar{\mathscr{R}}$, is the same as equation (5.9) of reference [5]. (Note that $\bar{\mathscr{R}} = 1$ for a hard walled duct) The normalized wall impedance ζ, which appears in this equation through the reflection coefficient $\bar{\mathscr{R}}$, must be evaluated at the actual (or observation) frequency

$$\omega = \omega_s/(1 - M_c\cos\theta_\infty), \tag{43}$$

and not the source frequency ω_s.

It is convenient to allow the transverse orientation of the quadrupoles to vary with source position. This amounts to changing the orientation of the $\mathbf{x}^s$ co-ordinate system or, equivalently, referencing the angle λ to a different angle, say $\lambda_0(\mathbf{x}^s)$. Then it follows from the results given in reference [5] that σ_2 and σ_3 are given explicitly by

$$\sigma_2 = \frac{q_s \cos(\lambda - \lambda_0)}{1 - M_c \cos\theta_\infty}, \quad \sigma_3 = \frac{q_s \sin(\lambda - \lambda_0)}{1 - M_c \cos\theta_\infty}, \tag{44}$$

where

$$q \equiv \sqrt{\frac{(1 - M\cos\theta_\infty)^2}{(\bar{c}/\bar{c}_\infty)^2} - \cos^2\theta_\infty}. \tag{45}$$

When multiple rays (which we individuate by a superscript in parentheses) reach the observer the far-field pressure is given by the somewhat more complicated formula

$$|p|^2 \to \frac{k_s^4 Q_{ij} Q_{kl}^* D_{ijkl}}{(4\pi R)^2 \bar{c}_\infty^2 \bar{c}_s^2 \ (1 - M_s\cos\theta_\infty)^2 (1 - M_c\cos\theta_\infty)^2}, \tag{46}$$

where $*$ denotes the complex conjugate, and the dependence on the transverse source coordinates, r_s, ϕ_s, and the emission angle λ enters through

$$D_{ijkl} \equiv \sum_{n,m=1}^{\kappa} \sigma_i^{(n)} \sigma_j^{(n)} \sigma_k^{(m)} \sigma_l^{(m)} \bar{\mathscr{R}}^{(n)} \bar{\mathscr{R}}^{(m)*} \sqrt{\left|\frac{\partial\lambda^{(n)}}{\partial\phi_\infty}\right| \left|\frac{\partial\lambda^{(m)}}{\partial\phi_\infty}\right|} \, \mathrm{e}^{\mathrm{i}(\omega/\bar{c}_\infty)(S_0^{(n)} - S_0^{(m)})}, \tag{47}$$

where κ denotes the number of rays reaching the observer.

3. REDUCTION OF ORDER OF RAY EQUATIONS

Goldstein [5] introduced the two-dimensional ray distance $\mathscr{S}$ defined by (see equation (2.19) of that reference)

$$\left|\frac{\mathrm{d}\mathbf{x}_t}{\mathrm{d}\mathscr{S}}\right| = 1. \tag{48}$$

It follows from equations (9), the first of equations (13), (28) and (45), that τ is related to $\mathscr{S}$ by

$$\frac{\mathrm{d}\mathscr{S}}{\mathrm{d}\tau} = q. \tag{49}$$

Equations (13) can then be combined to obtain the second-order system

$$\frac{\mathrm{d}}{\mathrm{d}\mathscr{S}} \, q \, \frac{\mathrm{d}\mathbf{x}_t}{\mathrm{d}\mathscr{S}} = \nabla_t q, \tag{50}$$

where ∇_t denotes the cross stream divergence. This is the same as equation (2.23) of reference [5], where it is shown, by introducing the polar co-ordinates

$$\phi = \tan^{-1}(x_3/x_2), \quad r = \sqrt{x_2^2 + x_3^2}, \tag{51}$$

that it can be reduced to the single second-order equation

$$\frac{1}{I}\frac{\mathrm{d}}{\mathrm{d}\phi}\frac{r^2 q}{I} = \frac{\partial q}{\partial \phi}, \tag{52}$$

where

$$I \equiv \sqrt{r^2 + \left(\frac{\mathrm{d}r}{\mathrm{d}\phi}\right)^2}, \tag{53}$$

which is to be solved subject to the initial conditions

$$r = r_s; \quad \frac{\mathrm{d}r}{\mathrm{d}\phi} = r_s \cot(\lambda - \phi_s) \text{ at } \phi = \phi_s, \tag{54}$$

where ϕ_s is the circumferential angle of the source point.

Inserting equations (13) and (49) into the boundary condition (23), using equation (51) and taking ϕ as the independent variable, shows that the appropriate boundary condition for equation (52) is

$$\frac{1}{I_+}\left[\frac{\mathrm{d}r_+}{\mathrm{d}\phi} - r_+ \tan(\phi - \beta)\right] = \frac{1}{I_-}\left[\frac{\mathrm{d}r_-}{\mathrm{d}\phi} - r_- \tan(\phi - \beta)\right] \quad \text{for } \mathbf{x} \text{ on } \Sigma, \tag{55}$$

where we have put

$$\hat{\mathbf{n}} \equiv \{\cos\beta, \sin\beta\}. \tag{56}$$

This boundary condition must be imposed on all rays reaching the cylindrical surface containing the duct wall whenever

$$x_1 \leqslant x_e(x_2, x_3), \tag{57}$$

where $x_1 = x_e(x_2, x_3)$ is the equation for the termination curve C. x_1 can be calculated as a function of ϕ along the ray by inserting equations (28), (49), (51), and (53) into equation (12) to obtain

$$\frac{\mathrm{d}x_1}{\mathrm{d}\phi} = \frac{I}{q}\left(\frac{\bar{c}_\infty}{\bar{c}}\right)^2 \left\{\left[\left(\frac{\bar{c}}{\bar{c}_\infty}\right)^2 - M^2\right]\cos\theta_\infty + M\right\}. \tag{58}$$

4. APPLICATION TO SOUND RADIATED BY ACTUAL TURBULENT FLOWS

Equations (46) and (47) can be used to calculate the power spectral density of a spectral distribution of sources of band width $\Delta\omega_s$ by putting $Q_{ij}Q^*_{kl}$ equal to $(1 - M_c \cos\theta_\infty)$ $\Psi_{ijkl}\Delta\omega_s$ [11]. However, pressure spectra are measured per unit observation frequency $\Delta\omega$:

$$\Delta\omega = \frac{\Delta\omega_s}{1 - M_c \cos\theta_\infty} \tag{59}$$

(see equation (43)) and it therefore follows that the directivity of the spectra at constant source frequency ω_s (due to a source at $\mathbf{x}^s$) is given by

$$\frac{1}{\Delta\omega}|p|^2 \to \frac{k_s^4 \Psi_{ijkl} D_{ijkl}}{(4\pi R)^2 \bar{c}_s^2 \bar{c}_\infty^2 (1 - M_s \cos\theta_\infty)^2}. \tag{60}$$

This result can now be used to calculate the sound emitted by an actual turbulent flow by assuming that the turbulent eddies behave like compact sound sources, and using Lilley's equation to show that the spectral source strength Ψ_{ijkl} is related to the fourth-order, two-point, time-delayed correlation function of the turbulence,

$$R_{ijkl}(\mathbf{x}^s, \boldsymbol{\xi}, \tau) = \overline{u_i' u_j' u_k'' u_l''} - \overline{u_i' u_j'}\ \overline{u_k'' u_l''}, \tag{61}$$

in the usual way by

$$\Psi_{ijkl} = \int_{-\infty}^{\infty}\int e^{i\omega_s \tau} R_{ijkl}(\mathbf{x}^s, \boldsymbol{\xi}, \tau)\, d\boldsymbol{\xi}\, d\tau, \tag{62}$$

where the single prime indicates that the quantity is evaluated at the position and time $(\mathbf{x}^{s\prime}, t)$, the double prime indicates the position and time $(\mathbf{x}^{s\prime\prime}, t + \tau)$,

$$\boldsymbol{\xi} = \mathbf{x}^{s\prime\prime} - \mathbf{x}^{s\prime} - \hat{\mathbf{i}} U_c \tau \tag{63}$$

and

$$\mathbf{x}^s = \{x_1^{s\prime}, \tfrac{1}{2}(x_2^{s\prime} + x_2^{s\prime\prime}), \tfrac{1}{2}(x_3^{s\prime} + x_3^{s\prime\prime})\} \tag{64}$$

denotes the mean position of the source.

Since the sound field is always produced by a distribution of sources rather than by single point source, the final result will involve an integral of equation (60) (and consequently of equation (47)) over the transverse source co-ordinates r_s and ϕ_s. Then, since $S_0^{(n)}$ is a function of these co-ordinates, the contribution from the cross-coupling terms in equation (47) will be smaller than the contribution of the $m = n$ terms by a factor of (at least) $\omega^{-1/2}$, which in a strict asymptotic sense is negligible in the high-frequency limit. However, the zero-mean-flow computations by Boyd *et al.* [12] suggest that the asymptotic convergence may be relatively slow for sources close to the wall (which result in small values of $S_0^{(n)} - S_0^{(m)}$ in equation (47)), and that the interference effects may not be insignificant even at relatively high frequencies—particularly at smaller angles to the downstream axis where the sound field is expected to be maximal. However, the turbulent flows which are of interest here, will probably introduce significant random fluctuations in the phases of the disturbances, which will tend to uncorrelate the pressure fluctuations corresponding to different ray paths. We therefore feel that it is best to neglect the interference effects, which amounts to replacing equation (47) by

$$D_{ijkl} = \sum_{n=1}^{\kappa} \sigma_i^{(n)} \sigma_j^{(n)} \sigma_k^{(n)} \sigma_l^{(n)} |\bar{\mathscr{R}}^{(n)}|^2 \left|\frac{\partial \lambda^{(n)}}{\partial \phi_\infty}\right|. \tag{65}$$

Since the fourth-order correlation tensor is very difficult to measure experimentally, or even calculate numerically, it is usual to assume that the turbulence is quasi-normal and, consequently, that R_{ijkl} can be expressed as the product of second-order correlations

[13, 14]

$$R_{ijkl} = R_{ik}R_{jl} + R_{il}R_{jk}. \tag{66}$$

In order to simplify this further, Goldstein and Rosenbaum [15], Kerschen [16] and, more recently, Béchara *et al.* [17] and Khavaran [18], assumed that the turbulence is axisymmetric about the direction of the mean flow. The analysis given in reference [1] (see also Dill *et al.* [2]) then shows that

$$\sigma_i\sigma_j\sigma_k\sigma_l\Psi_{ijkl} = 2\left\{|\boldsymbol{\sigma}|^4\int_{-\infty}^{\infty}\int e^{i\omega_s\tau}\bar{Q}_0\,d\xi\,d\tau - 2(\sigma_2\sigma_3)^2\int_{-\infty}^{\infty}\int e^{i\omega_s\tau}(\bar{Q}_{23}-\bar{Q}_{22})\,d\xi\,d\tau\right.$$

$$\left. + \sigma_i^2\sigma_j^2\int_{-\infty}^{\infty}\int e^{i\omega_s\tau}\bar{Q}_{ij}\,d\xi\,d\tau\right\}, \tag{67}$$

where we have dropped the superscript (n) on the σ_i, and

$$\bar{Q}_{11} = R_{11}^2 - R_{12}^2, \quad \bar{Q}_{12} = \bar{Q}_{13} = R_{12}^2 + R_{11}R_{22},$$
$$\bar{Q}_{22} = \bar{Q}_{33} = R_{22}^2 - R_{12}^2, \quad \bar{Q}_{23} = R_{22}^2 - R_{23}^2, \quad \bar{Q}_0 = R_{12}^2, \tag{68}$$

are symmetric in their indices.

5. APPLICATION TO ROUND DUCT WITH AXISYMMETRIC MEAN FLOW

Reference [5] shows that equations (52)–(54) can be solved analytically when the mean flow is axisymmetric. A similar procedure can be used to obtain an analytical solution to the present problem, but it is probably easier to solve it numerically. However, it is important to notice that in this case the resulting solution, whether obtained analytically or numerically, will depend on λ, ϕ and ϕ_s only in the combinations ϕ–ϕ_s and $\lambda - \phi_s$, since the coefficient q in equation (52) is independent of ϕ, i.e., ϕ appears only as an independent variable. This, in particular, implies that $\lambda - \phi_s$ is a function of $\phi_\infty - \phi_s$, r_s and θ_∞. Moreover, calculations of the ray trajectories for sources located within the nozzle show that λ is a discontinuous, multi-valued function of ϕ_∞, due to the sudden change of boundary conditions at the nozzle lip. This is illustrated in Figure 2, which is a plot of ϕ_∞ versus λ for the indicated source location. Thus, even though ϕ_∞ is necessarily a single-valued function of λ, the figure shows that the converse is certainly not true.

These observations can be used to simplify the calculation of the sound spectral density due to a ring source of radius r_s, which is often used as source model in axisymmetric jets. The ring source solution involves evaluation of integrals of the form

$$\int_0^{2\pi}\sin^p(\lambda^{(n)}-\phi_s)\cos^q(\lambda^{(n)}-\phi_s)\,|\bar{\mathscr{R}}^{(n)}|^2\left|\frac{d\lambda^{(n)}}{d\phi_\infty}\right|d\phi_s, \tag{69}$$

for $p, q = 0, 1, 2$, which, *for polar angles at which all emitted rays reach the far field*, can be written as

$$\int_0^{2\pi}\sin^p(\lambda^{(n)}-\phi_s)\cos^q(\lambda^{(n)}-\phi_s)\,|\bar{\mathscr{R}}^{(n)}|^2\left|\frac{d(\lambda^{(n)}-\phi_s)}{d\phi_s}\right|d\phi_s$$

$$= \int_0^{2\pi}\sin^p\bar{\lambda}^{(n)}\cos^q\bar{\lambda}^{(n)}\,|\bar{\mathscr{R}}^{(n)}|^2\,d\bar{\lambda}^{(n)} \tag{70}$$

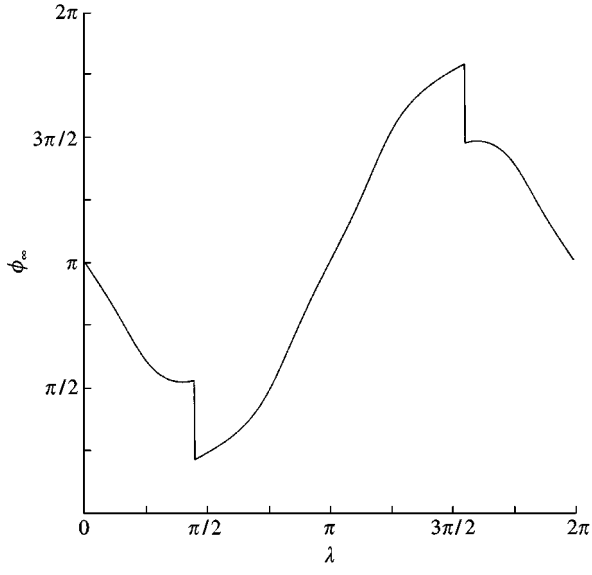

Figure 2. Farfield circumferential angle vs. initial circumferential angle for Mach number profile (72) with $a = 0{\cdot}1$, $b = 6$, $M(0) = 0{\cdot}9$ and source position $r_s = 0{\cdot}75r_0$, $x_1^s = -0{\cdot}5r_0$, and $\theta_\infty = 3\pi/8$.

since, for a given r_s and θ_∞, $\bar{\mathscr{R}}$ depends on $\phi_\infty - \phi_s$ only through $\lambda - \phi_s$. The integrals in equation (70) must be summed over all $\lambda^{(n)}$ values corresponding to any given value of ϕ_∞, in order to account for all of the rays reaching a given observation point.

As shown by the numerical results presented in the next subsection, some of the rays are cut off by the duct when the far-field polar angle θ_∞ becomes sufficiently large, in which case the last integration in equation (70) should be confined to those rays that reach the far field.

If we now choose the reference angle λ_0 in equation (44) to be equal to ϕ_s, the quadrupole sources will have the same orientation relative to the radial direction for all ϕ_s, i.e., the quadrupole source distribution in equation (60) will be axisymmetric when Ψ_{ijkl} is independent of ϕ_s. Then, since equations (44), (45), (65), and (67) show that the entire ϕ_∞ dependence in equation (60) is of the form (69), it follows that the sound field emitted by a ring of uncorrelated, equi-strength quadrupole sources with radius r_s, and the same orientation relative to the radial direction, is independent of the circumferential observation angle ϕ_∞, i.e., it is axisymmetric.

When $|\bar{\mathscr{R}}| = 1$ (i.e., for a hard-walled duct) and when all rays reach the far field, it follows from equations (44), (45), (67), (69) and (70) that

$$\sum_{n=1}^{\kappa} \int_0^{2\pi} \sigma_i^{(n)} \sigma_j^{(n)} \sigma_k^{(n)} \sigma_l^{(n)} \Psi_{ijkl} |\bar{\mathscr{R}}^{(n)}|^2 \left| \frac{\partial \lambda^{(n)}}{\partial \phi_\infty} \right| \mathrm{d}\phi_s$$

$$= \frac{4\pi}{(1 - M_c \cos\theta_\infty)^4} \left[q_s^4 \int_{-\infty}^{\infty} \int \mathrm{e}^{\mathrm{i}\omega_s \tau} (\bar{Q}_0 + \bar{Q}_{22}) \, \mathrm{d}\xi \, \mathrm{d}\tau \right.$$

$$+ 2q_s^2 \cos^2\theta_\infty \int_{-\infty}^{\infty} \int \mathrm{e}^{\mathrm{i}\omega_s \tau} (\bar{Q}_0 + \bar{Q}_{12}) \, \mathrm{d}\xi \, \mathrm{d}\tau$$

$$\left. + \cos^4\theta_\infty \int_{-\infty}^{\infty} \int \mathrm{e}^{\mathrm{i}\omega_s \tau} (\bar{Q}_0 + \bar{Q}_{11}) \, \mathrm{d}\xi \, \mathrm{d}\tau \right]. \tag{71}$$

This means that the sound radiated by a ring source in a hard-walled duct is not only independent of the mean velocity profile within the jet, but is also unaffected by the presence of the duct for the far-field polar angles at which all rays reach the far field. Of course, this result only applies when the phase cancellation between multiple rays can be neglected. Also, since $r_s \mathrm{d}\phi_s$ is the element of arc length, the total sound radiated by the ring source will be directly proportional to the radius r_s.

For isotropic turbulence $\bar{Q}_{ij} = 7\bar{Q}_0$, and it follows from equation (45) that equation (71) is independent of θ_∞ when $M_s = M_c$.

5.1. NUMERICAL RESULTS

Results for the directivity patterns due to a ring source within a round duct were computed for a constant mean speed of sound, $\bar{c} \equiv \bar{c}_\infty$, and mean Mach number profiles of the form

$$M(r) = M_0 \frac{\mathrm{e}^{-ar^b} - e^{-a}}{1 - \mathrm{e}^{-a}}, \tag{72}$$

where M_0 is the centerline Mach number and the parameters a and b are used to control the profile shape.

The source terms in equation (67) were evaluated using the relations given by Khavaran [18] for axisymmetric turbulence. The anisotropy is characterized by the two parameters $\overline{u_2^2}/\overline{u_1^2}$ and L_2/L_1, where $\overline{u_1^2}$ and $\overline{u_2^2}$ are the streamwise and transverse mean square turbulent velocities, respectively, and L_1 and L_2 are the corresponding correlation lengths (see Khavaran [18]). Values for the anisotropy parameters of $\overline{u_2^2}/\overline{u_1^2} = 0{\cdot}6$ and $L_2/L_1 = 0{\cdot}5$ were used in the calculations.

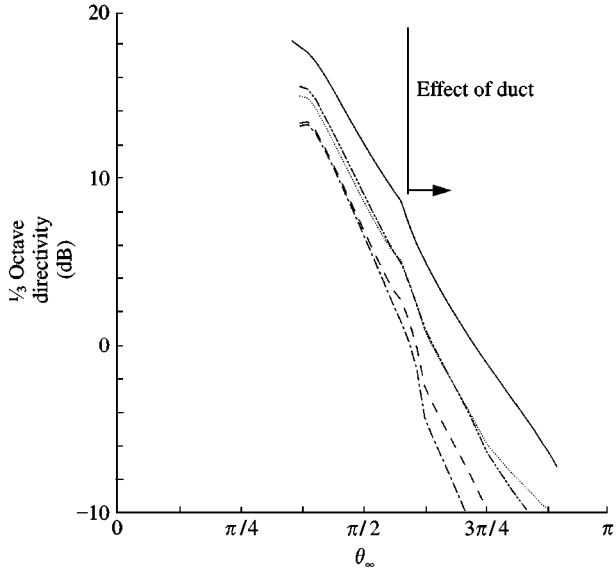

Figure 3. Farfield one-third-octave directivity plotted at constant source frequency for Mach number profile (72) with $a = 0{\cdot}1$, $b = 6$, $M(0) = 1{\cdot}5$, and source position $r_s = 0{\cdot}75r_0$, $x_1^s = -2{\cdot}0r_0$: ——, hard wall; – – – –, $\zeta = (1, -1)$; ...., $\zeta = (1/2, -1)$; –·–·–, $\zeta = (2, -1)$; –··–, $\zeta = (1, -2)$.

Figure 3 shows the results for the far field, one-third-octave directivity, plotted at constant source frequency, for a ring source at $r_s = 0{\cdot}75r_0$, $x_1^s = -2{\cdot}0r_0$, where r_0 is the duct radius, and a centerline Mach number of 1·5 with $a = 0{\cdot}1$, $b = 6$, for a hard-walled duct and a soft-walled duct of various impedances.

For sufficiently small far-field polar angles outside the zone of silence, all rays emanating from the source reach the far field and, for the perfectly reflecting, hard-walled duct considered here, the duct has no effect on the far-field sound. At far-field positions beginning in the upstream quadrant (i.e., $\theta_\infty > \pi/2$), however, some of the rays become trapped within the duct, causing the sound pressure levels to be reduced at these angles. The hard-walled duct, therefore, only effects the sound field at sufficiently large angles to the downstream axis which, in fact, lie in the upstream quadrant as indicated in the figure. Since the number of rays reaching the far field rapidly decreases as $\theta_\infty \to \pi$, there is a sharp drop in the far-field sound.

However, the soft-walled duct starts to effect the sound field as soon as wall reflections begin. Since an increasing number of rays reflect (an increasing number of times) off the walls as the polar angle increases there is a substantial decrease in the far-field sound relative to the hard-wall case. The wall impedances $\zeta = (1, -1)$ and $\zeta = (2, -1)$ are seen to reduce the peak noise level by nearly 5 dB, relative to the hard-wall case. The results suggest that the magnitude and phase of the normalized wall impedance can significantly effect the peak sound level, and a detailed parameter study to find the optimal value should be carried out.

Figures 4 and 5 show the effect of the source position on the far-field sound. The rays undergo fewer wall reflections when the source is closer to the nozzle exit (Figure 4), and the acoustic linear therefore provides less noise suppression. When the source is closer to the duct centerline (Figure 5), all rays exit the duct without reflecting off the wall when the far-field polar angle is sufficiently small, and the acoustic liner has no effect on the sound field. Wall reflections start to occur when the polar angle is increased, and the liner reduces the far-field sound, but only by a relatively small amount–again due to fewer wall reflections.

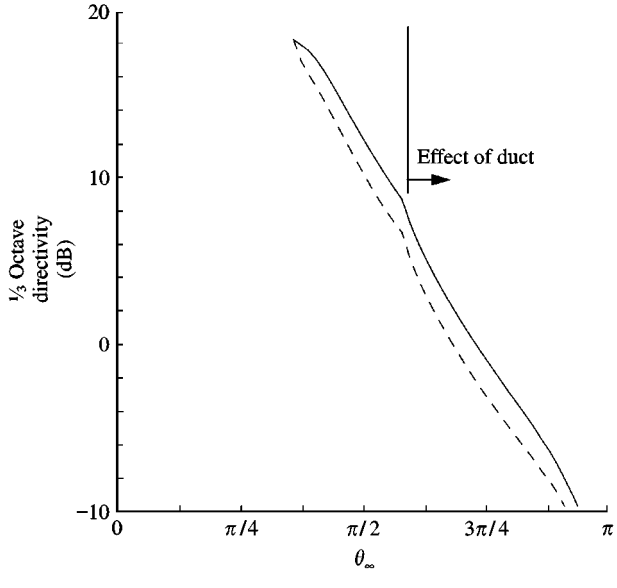

Figure 4. Farfield one-third-octave directivity plotted at constant source frequency for Mach number profile (72) with $a = 0{\cdot}1$, $b = 6$, $M(0) = 1{\cdot}5$, and source position $r_s = 0{\cdot}75r_0$, $x_1^s = -0{\cdot}5r_0$: ——, hard wall; – – – –, $\zeta = (1, -1)$.

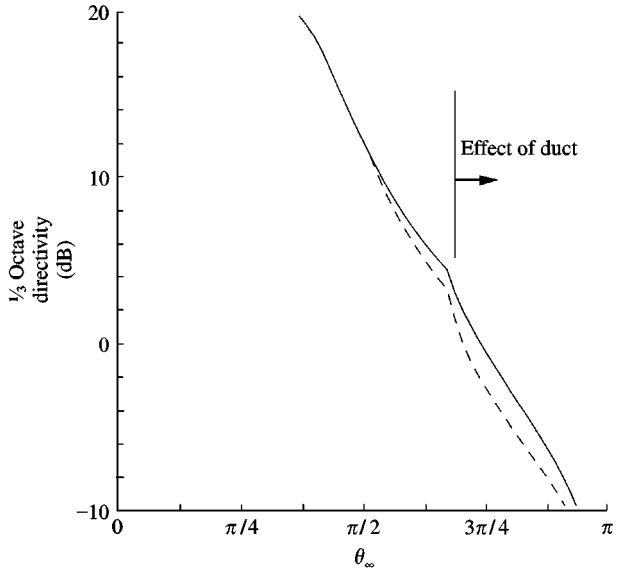

Figure 5. Farfield one-third-octave directivity plotted at constant source frequency for Mach number profile (72) with $a = 0{\cdot}1$, $b = 6$, $M(0) = 1{\cdot}5$, and source position $r_s = 0{\cdot}5r_0$, $x_1^s = -0{\cdot}5r_0$: ——, hard wall; – – – –, $\zeta = (1, -1)$.

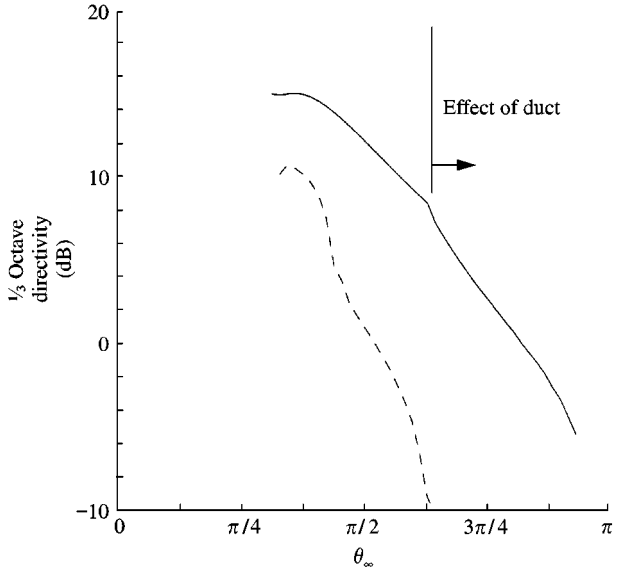

Figure 6. Farfield one-third-octave directivity plotted at constant source frequency for Mach number profile (72) with $a = 0{\cdot}1$, $b = 6$, $M(0) = 0{\cdot}9$, and source position $r_s = 0{\cdot}5r_0$, $x_1^s = -2{\cdot}0r_0$: ——, hard wall; – – – –, $\zeta = (1, -1)$.

Figure 6 illustrates the effect of centerline Mach number on the liner effectiveness. At the subsonic Mach number ($M(0) = 0{\cdot}9$) for which this result was obtained, a wall impedance of $\zeta = (1, -1)$ again reduces the peak sound pressure level by about 5 dB, but produces a much larger reduction than the previous (supersonic) case at large upstream angles.

6. CONCLUSIONS AND DISCUSSION

It was shown that the high-frequency Lilley's-equation solution developed in reference [5] for a doubly infinite, transversely sheared mean flow also applies to the noise generated internally within a nozzle, provided appropriate boundary conditions are imposed on the ray trajectories at the surface of the duct and a suitable wall impedance factor is included.

By assuming the turbulence to be axisymmetric about the mean flow direction, a simplified expression for the far-field sound radiated by a turbulent flow within the nozzle was derived.

The analysis was applied to the case of a round duct with an axisymmetric mean flow, and it was shown that a hard-walled duct has no effect on the farfield sound radiated at polar angles (outside the zone of silence) sufficiently close to the duct axis. The numerical results show that the duct cuts off some of the rays for polar angles in the upstream quadrant, and that acoustic liners can significantly reduce the farfield sound, but their effectiveness depends upon the wall impedance, source position and mean flow field. The analysis can be used to carry out detailed parametric studies to find the optimal wall impedance, acoustic source distributions, mean profile shape and nozzle geometry for a given application.

The ray acoustics solution has the advantage of being applicable to nozzles to any shape and any mean velocity profile (see Figure 1). The high-speed civil transport was expected to use a rectangular mixer-ejector nozzle with a very complex mean velocity profile and acoustically treated walls. Future work will evaluate the ray acoustics solution for this geometry and make comparisons with some recent test data.

This paper does not address the issue of the diffracted radiation resulting from acoustic rays striking the duct lip. However, a systematic high-frequency ($k \to \infty$) asymptotic analysis of this problem reveals that diffraction effects produce a correction to the mean square pressure that is order $(1/k)$ smaller than the direct and reflected radiation considered in this paper. Since this is smaller than the contribution due to ray interference effects, which have already been neglected in the analysis, it does not make sense to retain these diffraction effects here. It is also worth noting that the neglected 'shear-noise' source term appearing in equation (4), as well as higher order terms in the geometric acoustics solution (6), could also contribute up to an $O(1/k)$ correction to the mean square pressure.

The analysis assumes that the axial mean flow velocity vanishes at the duct wall (as well as on its downstream extension). Alternatively, the mean flow could be reduced to zero through a thin boundary layer near the surface. In that case the impedance in the boundary condition (22) would be replaced by an effective impedance imposed at the boundary layer edge [19], which accounts for both the actual wall impedance and the boundary layer effects. The reflection coefficient then becomes

$$\mathscr{R} = \frac{\eta + \beta}{\eta - \beta}, \tag{73}$$

where $\beta = 1 - M_\delta \cos\theta_\infty$, with M_δ being the Mach number at the edge of the boundary layer. Also, the ray trajectories would be modified by passing through the infinitesimally thin shear layer that extends downstream of the duct wall.

ACKNOWLEDGMENT

The authors would like to thank Dr James Bridges of NASA Glenn Research Center for providing values of the wall impedance, Dr Abbas Khavaran of Dynacs Engineering Co. for

information on the mixer-ejector nozzle configuration and flow field and Dr David Wundrow of the Ohio Aerospace Institute for the asymptotic estimates of the diffraction effects and Dr Andrew Kempton of Rolls Royce Ltd. for his helpful suggestions.

REFERENCES

1. M. E. GOLDSTEIN and B. M. ROSENBAUM 1973 *NASA TN D*-7118. Emission of sound from turbulence convected by a parallel flow in the presence of solid boundaries.
2. L. H. DILL, A. A. OYEDIRAN and E. A. KREJSA 1998 *NASA TM* 1998-207421. Refraction of sound emitted near solid boundaries from a sheared jet.
3. R. MANI, P. R. GLIEBE and T. F. BALSA 1978 *FAA-RD*-76-79-II. High velocity jet noise source location and reduction.
4. T. F. BALSA 1976 *Journal of Fluid Mechanics* **74**, 193–208. The far field of high frequency convected singularities sheared flows, with an application to jet-noise reduction.
5. M. E. GOLDSTEIN 1982 *Journal of Sound and Vibration* **80**, 499–522. High frequency sound emission from moving point multipole sources embedded in arbitrary transversely sheared mean flows.
6. P. A. DURBIN 1983 *Journal of Sound and Vibration* **91**, 519–525. High frequency Green function for aerodynamic noise in moving media, Part I: general theory.
7. P. A. DURBIN 1983 *Journal of Sound and Vibration* **91**, 527–538. High frequency Green function for aerodynamic noise in moving media, Part II: noise from a spreading jet.
8. M. E. GOLDSTEIN 1976 *Aeroacoustics*. New York: McGraw-Hill.
9. A. D. PIERCE 1981 *Acoustics*: *An Introduction to its Physical Principles and Applications*. New York: McGraw-Hill.
10. S. M. CANDEL 1977 *Journal of Fluid Mechanics* **83**, 465–493. Numerical solution of conservation equations arising in linear wave theory: application to aeroacoustics.
11. J. E. FFOWCS WILLIAMS 1963 *Philosophical Transactions of the Royal Society* **A255**, 469–503. The noise from turbulence convected at high speed.
12. W. K. BOYD, A. J. KEMPTON and C. L. MORFEY 1984 *Paper No. AIAA* 84-2332, *Presented at the American Institute of Aeronautics and Astronautics* 9*th Aeroacoustics Conference*, *Williamsburg*, *VA*, 15–17 October. Ray-theory predictions of the noise radiated from aero-engine ducts.
13. M. D. MILLIONSCHIKOV 1941 *Doklady Akademii Nauk. SSR* **32**, 611–614. Theory of homogeneous isotropic turbulence.
14. G. K. BATCHELOR 1953 *Theory of Homogeneous Turbulence*. Cambridge: Cambridge University Press.
15. M. E. GOLDSTEIN and B. M. ROSENBAUM 1973 *Journal of the Acoustical Society of America* **54**, 630–645. Effect of anisotropic turbulence on aerodynamic noise.
16. E. J. KERSCHEN 1983 *AIAA Journal* **21**, 978–985. Constraints on the invariant functions of axisymmetric turbulence.
17. W. BÉCHARA, P. LAFON, C. BAILLY and S. M. CANDEL 1995 *Journal of the Acoustical Society of America* **97**, 3518–3531. Application of a κ–ε turbulence model to the prediction of noise for simple and coaxial free jets.
18. A. KHAVARAN 1999 *AIAA Journal* **37**, 832–841. On the role of anisotropy in turbulent mixing noise.
19. M. E. GOLDSTEIN and E. RICE 1973 *Journal of Sound and Vibration* **30**, 79–84. Effect of shear on duct wall impedance.